Inorganic Chemistry

Forum Article

pubs.acs.org/IC

Frontier Orbital Engineering of Metal–Organic Frameworks with Extended Inorganic Connectivity: Porous Alkaline-Earth Oxides

Christopher H. Hendon,*[,†] Aron Walsh,[‡,§] and Mircea Dincă*[,†]

[†]Department of Chemistry, Massachusetts Institute of Technology, Cambridge, Massachusetts 02139, United States

[‡]Department of Chemistry, University of Bath, Bath BA2 7AY, U.K.

[§]Global E[3] Institute and Department of Materials Science and Engineering, Yonsei University, Seoul 120-749, Korea

ABSTRACT: The development of conductive metal–organic frameworks is challenging owing to poor electronic communication between metal clusters and the organic ligands that bridge them. One route to overcoming this bottleneck is to extend the inorganic dimensionality, while using the organic components to provide chemical functionality. Using density functional theory methods, we demonstrate how the properties of the alkaline-earth oxides SrO and BaO are transformed upon formation of porous solids with organic oxygen sources (acetate and trifluoroacetate). The electron affinity is significantly enhanced in the hybrid materials, while the ionization potential can be tuned over a large range with the polarity of the organic moiety. Furthermore, because of their high-vacuum fraction, these materials have dielectric properties suitable for low-κ applications.

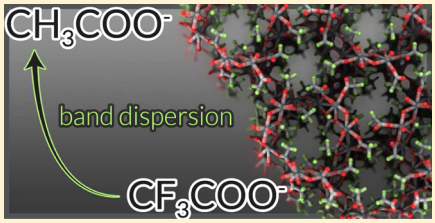

INTRODUCTION

Dense ionic solids have historically found applications in areas such as heterogeneous catalysis, energy conversion, and optics.[1,2] The rise of metal–organic frameworks (MOFs),[3] hybrid perovskites,[4,5] and other mixed colvalent-ionic systems[6,7] has expanded chemical space to a variety of new materials that boast an array of exciting properties including ionic[8] and electronic conductivity,[9−11] gas storage,[12] absorbate-induced piezochromism,[13] and magnetoelastic coupling.[14]

Many interesting physical properties of hybrid solids have been attributed to the electronic structure of the ligand (e.g., long-range magnetic coupling,[15] electron hopping,[16] and large pore volumes[17]). One byproduct of many designer ligands is an inherent porosity of the bulk material.[18] However, with porosity often comes a decrease in the electronic communication (orbital overlap) between the inorganic clusters, limiting the possibility of band transport and reducing the potential for application in electrical devices. There are rare examples where the ligand/metal interface forms a good ohmic contact, and these systems demonstrate high electrical conductivity.[19] The design of hybrid materials that feature periodic arrays of empty space *and* conduct electricity is paramount for next-generation metal–organic electronics.

3D inorganic connectivity (i.e., I^3O^0 following the notation of Cheetham, Rao, and Feller)[20] may be used as a descriptor for the discovery of porous conducting variations of the parent oxide, on the premise that extended inorganic connectivity may yield a continuous path for electron transport. For example, organic–inorganic halide perovskites are excellent semiconductors owing to the 3D network of corner-sharing metal halide octahedra; however, other examples are limited. Recently, Rabuffetti and colleagues reported two isostructural porous hybrid Sr^{2+} and Ba^{2+} oxide materials.[21] The solids ($Sr(CF_3COO)_2$ and $Ba(CF_3COO)_2$) were found to crystallize in the $R\bar{3}$ trigonal space group (Figure 1a), with 3D octomeric inorganic rings composed of edge-sharing metal oxides (Figure 1b) suspended by organic anions. The structures are topologically similar to the succinate compounds presented by Cheetham and co-workers.[22,23] Each metal ion exhibits an eight-coordinate environment, connected to six unique CF_3COO^- molecules (shown in Figure 1c). Given their topology, compositional similarity to the extensively studied parent oxides (SrO and BaO), and modularity of the organic linkage, we pursued $Sr(CF_3COO)_2$ and $Ba(CF_3COO)_2$ as candidates for widening our design principles for the formation of electroactive porous hybrid materials.

In this Forum Article, we use first-principles electronic structure calculations to elucidate the electronic band structures of $Sr(CF_3COO)_2$ and $Ba(CF_3COO)_2$ and demonstrate that the band positions and dispersions are dependent on the charge identity of the ligand. Owing to the 3D inorganic connectivity, the origin of this effect is more subtle than that in typical MOFs (I^0O^3 as found in materials like MOF-5,[26] MIL-125,[27] HKUST-1,[19] and MFU-4*l*[28]), where the inorganic regions are spatially separated by organic linkers in all three directions. We show that, in both the Sr^{2+} and Ba^{2+} compounds, the electronic band structure is modular and can be controlled by the anion. These materials feautre desirable chemical bonding and near-unity dielectric constants, making them of interest for low-κ applications in microelectronics.[29−31]

Special Issue: Metal-Organic Frameworks for Energy Applications

Received: April 21, 2016
Published: June 7, 2016

DOI: 10.1021/acs.inorgchem.6b00979
Inorg. Chem. 2016, 55, 7265−7269

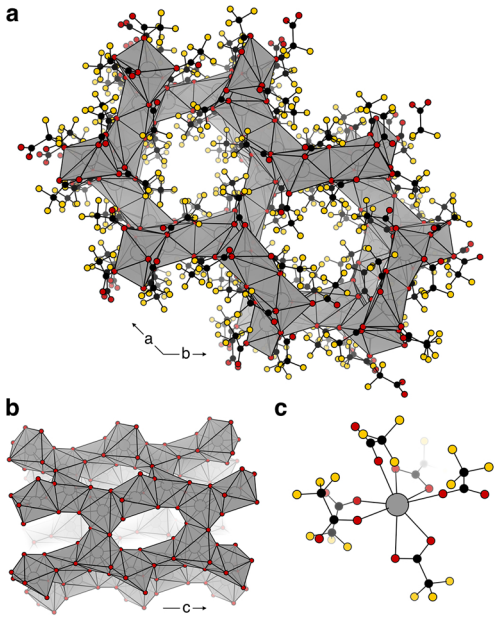

Figure 1. $Sr(CF_3COO)_2$ and $Ba(CF_3COO)_2$, which crystallize isostructurally in space group $R\bar{3}$ (a). Materials featuring 3D inorganic connectivity through octomeric metal oxide edge-sharing channels (b). Each metal being pseudooctahedral and eight-coordinate to six unique ligands (c). Carbon, oxygen, fluorine, and the metal are depicted in black, red, yellow, and gray, respectively.

Starting from the crystal structures determined from X-ray diffraction, the unit cell and internal positions were optimized using density functional theory (DFT), as detailed in the Computational Methods section. The resulting electronic band structures and projected density of states (pDOS) of $Sr(CF_3COO)_2$ and $Ba(CF_3COO)_2$ are presented in Figure 2 based on the HSE06 hybrid exchange-correlation functional. The work functions (solid-state ionization potentials) of the parent oxides were taken from a recent DFT study.[25] The parent oxides feature valence- and conduction-band edges centered on the O p and metal s orbitals, respectively.[32−36] This spatial charge separation is one requirement for long charge-carrier lifetimes. In the metal oxides, the oxygen ions carry a formal 2− charge, and the hybrid materials feature oxygen with an effective charge of 0.5−.

The highest occupied electronic states in both the parent oxide and hybrid materials are determined by the O and C p states, but CF_3COO^- has a significantly reduced charge density compared to O^{2-}. Because of charge delocalization over the organic π system, the O p states are stabilized [i.e., increased work function from 5.3 eV (4.2 eV) to 8.9 eV (8.8 eV) for $Sr(CF_3COO)_2$ ($Ba(CF_3COO)_2$)]. Unlike the parent oxides, whose conduction-band minima (CBM) are defined by metal s orbitals, the hybrid material ligand is able to accept an electron into the π system, and hence the CBM of $Sr(CF_3COO)_2$ and $Ba(CF_3COO)_2$ are primarily localized on the π oxygen and carbon atoms, resulting in a fundamental electronic gap defined by a ligand-to-ligand transition.

The magnitude and localization of the anionic charge influences the depth of the local electrostatic potential and, in turn, the positions of the valence- and conduction-band extrema resulting from the crystal field. The metal coordination environment is also important because it determines the polarity of the metal−ligand interaction. The coordination environments in the hybrid and parent oxide materials are presented on the left-hand side of Figure 2. Despite the hybrid material being formally eight-coordinate [such a coordination is also observed in the compositionally similar $Ba(AcO)_2$, where AcO = acetate[37]], the environment can be thought of as pseudooctahedral. Colored coordination vectors are included in Figure 2 to draw a comparison between the hybrid and parent oxide structures. In both $Sr(CF_3COO)_2$ and $Ba(CF_3COO)_2$, two of the six ligands are bidentate, acting as an effective 1− charge anion, which differs from that of the other four ligands, which carry a 0.5− charge.

In the porous structures, the frontier electronic structure is ligand-localized. The valence bands show narrow bandwidth. The dispersion in the valence-band maxima (VBM) of $(Sr(CF_3COO)_2$ is 0.08 eV, while for $Ba(CF_3COO)_2$, it is 0.06 eV. The CBM exhibit slightly more curvature [Sr-

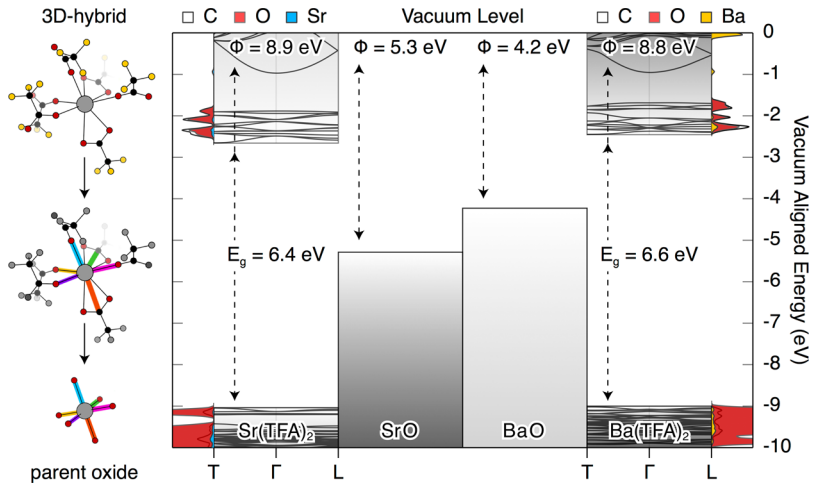

Figure 2. Similar electronic pDOS and band structures of $Sr(CF_3COO)_2$ and $Ba(CF_3COO)_2$, with the band extrema defined by the ligand O and C p orbitals. The porous structures differ from those of the parent oxides SrO and BaO, where the valence and conduction bands are defined by both O and C p and metal s orbitals, respectively.[24,25] The origin of this difference is due to both the change in the coordination environment (shown left) and the increase in the charge density in the parent oxide. The conduction band of BaO has been omitted for clarity because it is found to be 0.3 eV below the vacuum level, while SrO has a negative electron affinity. TFA = CF_3COO^-.

DOI: 10.1021/acs.inorgchem.6b00979
Inorg. Chem. 2016, 55, 7265−7269

$(CF_3COO)_2$ CBM dispersion = 0.17 eV; $Ba(CF_3COO)_2$ CBM dispersion = 0.07 eV]. While these values are large for MOFs (which typically range from 0 to 0.05 eV),[38,39] they are smaller than those of the parent oxide materials.

To support the postulation that charge-density fluctuations influence the electronic properties of these compounds, two new materials were constructed by trifluoroacetate (TFA)/acetate (AcO) substitutions. Although there are no reports of crystalline anhydrous $Sr(AcO)_2$, Gautier-Luneau and Mosset have reported an anhydrous $Ba(AcO)_2$ structure, and we considered $Sr(AcO)_2$ as isostructural to the Ba^{2+} compound.[37] Both structures feature the same pseudooctahedral coordination environment as that shown in Figure 2. The total energies of the hypothetical porous $Ba(AcO)_2$ and experimentally realized dense $Ba(AcO)_2$ were compared on the basis of DFT/HSE06 calculations. The hypothetical porous $Ba(AcO)_2$, shown in Figure 3, was found to be metastable (less stable by

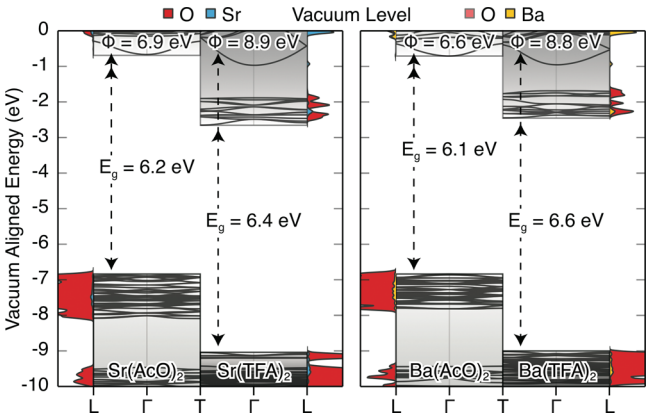

Figure 3. Inclusion of AcO = CH_3COO^- in the crystallographic TFA = CF_3COO^- positions, which increases the localization of charge on coordinating oxygen atoms and alters the absolute electron energies. Carbon contributions are omitted for clarity but feature contributions similar to those shown in Figure 2: VBM defined by primarily O p states, and CBM defined by equal contributions from the π system of oxygen and carbon atoms.

0.58 kcal/Ba^{2+}) relative to the dense anhydrous $Ba(AcO)_2$). The strontium-type materials exhibited comparable modularity. This is not unexpected because essentially all porous structures are less stable than their dense isomers,[40] and it suggests that a hypothetical porous $Ba(AcO)_2$ could be synthesized under appropriate conditions.

The charge densities of TFA and AcO are presented in Figure 4a. From these calculations, the AcO anion features a 25% increase in the oxygen charge density compared to that of the fluoronated analogue. The porous AcO anions are electronically distinct from the TFA analogues, as shown in Figure 3. AcO is a much stronger base than trifluoroacetic acid, $pK_a^{CF_3COOH}$ = 0.23 and pK_a^{AcOH} = 4.76, making AcO a stronger field ligand than TFA. This manifests as an increased valence-band energy (Figure 3). Furthermore, the band edges of the AcO anions no longer feature a ligand-to-ligand transition, as observed in TFA, but rather a ligand-to-metal transition, comparable to that in the parent oxides. When referenced to the vacuum level, the Ba s orbital remains unperturbed by the ligand identity (i.e., the bands have approximately the same energy levels).

To further explore the origin of the band reordering upon CF_3COO^-/CH_3COO^- substitution, the band structures for the

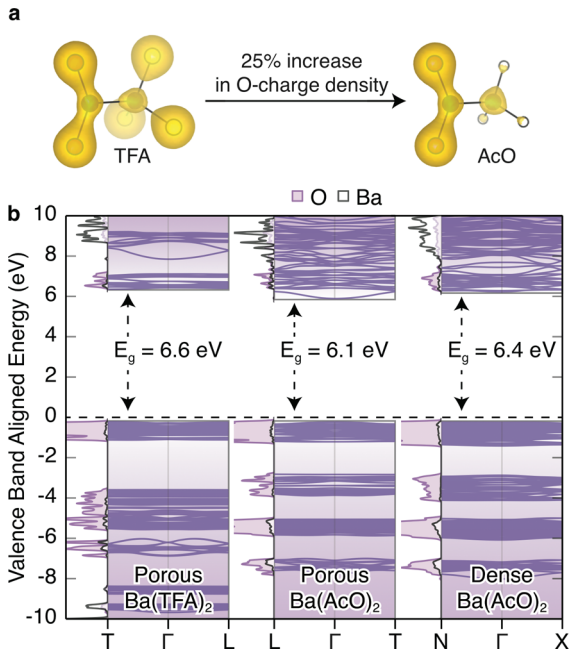

Figure 4. Charge density of the TFA^- and AcO^- ligands (a). The stronger base features a 25% increase in the relative oxygen charge density. The increase in the bandwidths is the product of a reordering of the band structure from ligand-to-ligand to ligand-to-metal transitions, as demonstrated in the comparison between $Ba(TFA)_2$ and dense $Ba(AcO)_2$ and theoretical porous $Ba(AcO)_2$ structures (b). The materials are aligned to their highest occupied states for comparison.

barium-type materials were aligned to their highest occupied states (Figure 4b). Strontium-type materials are not presented because of the absence of an experimentally realized anhydrous material. However, computations of the strontium-type hypothetical materials demonstrated trends comparable to those observed for the barium-type structures. The valence band is largely unaffected by the topology when compositionally identical materials [both porous and dense $Ba(AcO)_2$] are compared. The inclusion of TFA does not significantly alter the locality or density of the frontier valence bands.

Chemical substitution resulted in two other interesting changes in the electronic structure: (i) a shift from a $T \rightarrow T$ to a $\Gamma \rightarrow \Gamma$ fundamental electronic transition in the first Brillouin zone; (ii) a reordering of the conduction bands such that the localized ligand unoccupied states (formally found in the CF_3COO^- materials at ca. −2 eV) are increased in energy to above the vacuum level. Together, these cause a significant increase in the dispersion of the conduction band because of the CBM being defined by the metal s orbitals.

The enhancement of band dispersion based on simple chemical substitutions is evidence that the electronic properties of MOFs are intimately linked to the charge density of the ligand. When the O p character is increased, the MOF obtains a lower conduction band defined by metal s orbitals and accesses a parent oxide-like electronic structure. While the energy of the valence bands is augmented as a function of the oxygen charge density, the dispersion remains unperturbed.

Although the wide band gaps of these materials render them insulators in the absence of doping, there is an added benefit of porosity: low dielectric constants (ϵ_∞), which make porous $Sr(AcO)_2$ and $Ba(AcO)_2$ interesting candidates for blocking layers in electrical devices. Compared to the parent oxides

DOI: 10.1021/acs.inorgchem.6b00979
Inorg. Chem. 2016, 55, 7265−7269

(SrO, ϵ_∞ = 14.5;[41] BaO, ϵ_∞ = 34),[42] these porous structures feature near-unity optical dielectric constants (Table 1).

Table 1. Electronic Properties (DFT/HSE06) of the Four Porous Materials Considered Here[a]

material	IP (eV)	EA (eV)	E_g (eV)	ϵ_∞
$Sr(CH_3COO)_2$	6.9	0.7	6.2	1.51
$Sr(CF_3COO)_2$	8.9	2.5	6.4	1.72
$Ba(CH_3COO)_2$	6.6	0.5	6.1	1.77
$Ba(CF_3COO)_2$	8.8	2.2	6.6	1.77

[a]The ionization potential (IP; equivalent to the work function Φ for E_F = VBM], electron affinity (EA), and electronic band gap (E_g) are presented. The high-frequency dielectric constant (ϵ_∞) is also presented.

Reports of MOFs for blocking layers are sparse. To the best of our knowledge, only ZIF-8 has been postulated as a low-κ dielectric based on a dielectric constant of 2.3.[43] For reference, these are comparatively low relative to other hybrid materials ($CH_3NH_3PbI_3$, $\epsilon_\infty \sim 6$[44]).

In summary, we have demonstrated the changes in the chemical bonding and electronic structures that occur in alkaline-earth metal oxides upon a transition from dense to porous metal−organic structures. We have further shown that changing the charge density of the ligand alters the frontier crystalline orbital composition, band dispersion, and dielectric constants. These findings can be instructive for the design of conductive hybrid solids with tunable band structures.

COMPUTATIONAL DETAILS

First-principles total energy and electronic structure calculations were performed within the Kohn−Sham DFT construct. A delocalized plane-wave basis set with projector-augmented-wave scalar-relativistic frozen-core potentials was employed, as implemented in the Vienna ab initio simulation package (*VASP*).[45] A 500 eV plane-wave kinetic-energy cutoff and a 2 × 2 × 2 k grid were combined to provide total energy convergence to within 0.01 eV/atom. Beginning with the experimentally determined crystallographic cell, all unit cell vectors and internal ionic positions were relaxed to their equilibrium values using the PBEsol[46] functional. This functional provides a good description of the solid-state structures of MOFs, with all equilibrium lattice vectors being within 1% of the experimental values.

To recover more accurate electronic properties with a more sophisticated description of the quantum-mechanical electron−electron interactions, an additional optimization was required[47] using a hybrid exchange-correlation functional (HSE06), with 25% of the short-range semilocal exchange replaced by the nonlocal Hartree−Fock exchange.[48,49] This method was used to recover electronic properties including the electron density, band gap, and band structure. The k points sampled were determined by the high-symmetry points for the $R\bar{3}$ space group, as detailed in Figures 2 and 3. A 3 × 3 × 3 k grid was used to compute the high-frequency (optical) dielectric constants based on valence-to-conduction band transitions computed in the independent-particle approximation using Fermi's Golden rule.

In order to calculate the reference electrostatic potential (vacuum level), we take an average of the Hartree potential in the vacuum region of the cell and use this as an internal reference for the electronic eigenvalues.[50] The analysis code for this calculation, which can also calculate planar and macroscopic averages of electrostatic potentials and charge densities, is freely available.[51]

Single-molecule charge-density calculations were performed in FHI-aims,[52] using the same functionals, sufficiently large basis set, and convergence criteria as the periodic solid. The charge density was obtained using an electrostatic potential segmentation method.

Visualizations of the structures were made using *VESTA*, color scheme "Credit Union".[53]

AUTHOR INFORMATION

Corresponding Authors

*E-mail: hendon@mit.edu.

*E-mail: mdinca@mit.edu.

Notes

The authors declare no competing financial interest.

ACKNOWLEDGMENTS

M.D. and C.H.H. are supported by the U.S. Department of Energy, Office of Science, Office of Basic Energy Sciences (Award DE-SC0006937). This work used the Extreme Science and Engineering Discovery Environment, which is supported by National Science Foundation Grant ACI-1053575 and benefited from access to ARCHER, the U.K.'s national high-performance computing service, funded by the EPSRC (Grant EP/L000202). A.W. is supported by the EPSRC (Grant EP/M009580/1) and ERC (Grant 277757).

REFERENCES

(1) Protesescu, L.; Yakunin, S.; Bodnarchuk, M. I.; Krieg, F.; Caputo, R.; Hendon, C. H.; Yang, R. X.; Walsh, A.; Kovalenko, M. V. *Nano Lett.* **2015**, *15*, 3692−3696.

(2) Scanlon, D. O.; Dunnill, C. W.; Buckeridge, J.; Shevlin, S. A.; Logsdail, A. J.; Woodley, S. M.; Catlow, C. R. A.; Powell, M. J.; Palgrave, R. G.; Parkin, I. P.; Watson, G. W.; Keal, T. W.; Sherwood, P.; Walsh, A.; Sokol, A. A. *Nat. Mater.* **2013**, *12*, 798−801.

(3) James, S. L. *Chem. Soc. Rev.* **2003**, *32*, 276−288.

(4) Frost, J. M.; Butler, K. T.; Brivio, F.; Hendon, C. H.; van Schilfgaarde, M.; Walsh, A. *Nano Lett.* **2014**, *14*, 2584−2590.

(5) Brenner, T. M.; Egger, D. A.; Kronik, L.; Hodes, G.; Cahen, D. *Nat. Rev. Mater.* **2016**, *1*, 15007.

(6) Corma, A. *J. Catal.* **2003**, *216*, 298−312.

(7) Hendon, C. H.; Yang, R. X.; Burton, L. A.; Walsh, A. *J. Mater. Chem. A* **2015**, *3*, 9067−9070.

(8) Tominaka, S.; Cheetham, A. K. *RSC Adv.* **2014**, *4*, 54382−54387.

(9) Hendon, C. H.; Tiana, D.; Walsh, A. *Phys. Chem. Chem. Phys.* **2012**, *14*, 13120−13132.

(10) Talin, A. A.; Centrone, A.; Ford, A. C.; Foster, M. E.; Stavila, V.; Haney, P.; Kinney, R. A.; Szalai, V.; El Gabaly, F.; Yoon, H. P.; Léonard, F.; Allendorf, M. D. *Science* **2014**, *343*, 66−69.

(11) Sun, L.; Hendon, C. H.; Minier, M. A.; Walsh, A.; Dincă, M. *J. Am. Chem. Soc.* **2015**, *137*, 6164−6167.

(12) Rowsell, J. L. C.; Yaghi, O. M. *Angew. Chem., Int. Ed.* **2005**, *44*, 4670−4679.

(13) Hendon, C. H.; Wittering, K. E.; Chen, T.-H.; Kaveevivitchai, W.; Popov, I.; Butler, K. T.; Wilson, C. C.; Cruickshank, D. L.; Miljanić, O. Š.; Walsh, A. *Nano Lett.* **2015**, *15*, 2149−2154.

(14) Saines, P. J.; Barton, P. T.; Jura, M.; Knight, K. S.; Cheetham, A. K. *Mater. Horiz.* **2014**, *1*, 332−337.

(15) Tiana, D.; Hendon, C. H.; Walsh, A. *Chem. Commun.* **2014**, *50*, 13990−13993.

(16) Park, S. S.; Hontz, E. R.; Sun, L.; Hendon, C. H.; Walsh, A.; Van Voorhis, T.; Dincă, M. *J. Am. Chem. Soc.* **2015**, *137*, 1774−1777.

(17) Farha, O. K.; Wilmer, C. E.; Eryazici, I.; Hauser, B. G.; Parilla, P. A.; O'Neill, K.; Sarjeant, A. A.; Nguyen, S. T.; Snurr, R. Q.; Hupp, J. T. *J. Am. Chem. Soc.* **2012**, *134*, 9860−9863.

(18) Wilmer, C. E.; Leaf, M.; Lee, C. Y.; Farha, O. K.; Hauser, B. G.; Hupp, J. T.; Snurr, R. Q. *Nat. Chem.* **2011**, *4*, 83−89.

(19) Hendon, C. H.; Walsh, A. *Chem. Sci.* **2015**, *6*, 3674−3683.

(20) Cheetham, A. K.; Rao, C. N. R.; Feller, R. K. *Chem. Commun.* **2006**, 4780−4795.

(21) Dissanayake, K. T.; Mendoza, L. M.; Martin, P. D.; Suescun, L.; Rabuffetti, F. A. *Inorg. Chem.* **2016**, *55*, 170−176.

DOI: 10.1021/acs.inorgchem.6b00979
Inorg. Chem. 2016, 55, 7265−7269

(22) Forster, P. M.; Cheetham, A. K. *Angew. Chem., Int. Ed.* **2002**, *41*, 457−477.
(23) Forster, P. M.; Burbank, A. R.; Livage, C.; Ferey, G.; Cheetham, A. K. *Chem. Commun.* **2004**, 368−369.
(24) Junquera, J.; Zimmer, M.; Ordejon, P.; Ghosez, P. *Phys. Rev. B: Condens. Matter Mater. Phys.* **2003**, *67*, 155327.
(25) Logsdail, A. J.; Scanlon, D. O.; Catlow, C. R. A.; Sokol, A. A. *Phys. Rev. B: Condens. Matter Mater. Phys.* **2014**, *90*, 155106.
(26) Rosi, N. L.; Eckert, J.; Eddaoudi, M.; Vodak, D. T.; Kim, J.; O'Keeffe, M.; Yaghi, O. M. *Science* **2003**, *300*, 1127−1129.
(27) Hendon, C. H.; Tiana, D.; Fontecave, M.; Sanchez, C.; D'arras, L.; Sassoye, C.; Rozes, L.; Mellot-Draznieks, C.; Walsh, A. *J. Am. Chem. Soc.* **2013**, *135*, 10942−10945.
(28) Metzger, E. D.; Brozek, C. K.; Comito, R. J.; Dincă, M. *ACS Cent. Sci.* **2016**, *2*, 148−153.
(29) Hu, C.; Morgen, M.; Ho, P. S.; Jain, A.; Gill, W. N.; Plawsky, J. L.; Wayner, P. C., Jr *Appl. Phys. Lett.* **2000**, *77*, 145.
(30) Wang, Z.; Wang, H.; Mitra, A.; Huang, L.; Yan, Y. *Adv. Mater.* **2001**, *13*, 746−749.
(31) Shamiryan, D.; Abell, T.; Iacopi, F.; Maex, K. *Mater. Today* **2004**, *7*, 34−39.
(32) Broqvist, P.; Panas, I.; Fridell, E.; Persson, H. *J. Phys. Chem. B* **2002**, *106*, 137−145.
(33) Branda, M.; DiValentin, C.; Pacchioni, G. *J. Phys. Chem. B* **2004**, *108*, 4752−4758.
(34) Di Valentin, C.; Ferullo, R.; Binda, R.; Pacchioni, G. *Surf. Sci.* **2006**, *600*, 1147−1154.
(35) Duan, Y.; Qin, L.; Tang, G.; Shi, L. *Eur. Phys. J. B* **2008**, *66*, 201−209.
(36) Halim, W. A.; Assem, M.; Shalabi, A. S.; Soliman, K. *Appl. Surf. Sci.* **2009**, *255*, 7547−7555.
(37) Gautier-Luneau, I.; Mosset, A. *J. Solid State Chem.* **1988**, *73*, 473−479.
(38) Liu, J.; Zhou, W.; Liu, J.; Howard, I.; Kilibarda, G.; Schlabach, S.; Coupry, D.; Addicoat, M.; Yoneda, S.; Tsutsui, Y.; Sakurai, T.; Seki, S.; Wang, Z.; Lindemann, P.; Redel, E.; Heine, T.; Wöll, C. *Angew. Chem., Int. Ed.* **2015**, *54*, 7441−7445.
(39) Butler, K. T.; Hendon, C. H.; Walsh, A. *ACS Appl. Mater. Interfaces* **2014**, *6*, 22044−22050.
(40) Appelhans, L. N.; Kosa, M.; Radha, A.; Simoncic, P.; Navrotsky, A.; Parrinello, M.; Cheetham, A. K. *J. Am. Chem. Soc.* **2009**, *131*, 15375−15386.
(41) Samara, G. *Phys. Rev.* **1968**, *165*, 959−969.
(42) Bever, R. S.; Sproull, R. L. *Phys. Rev.* **1951**, *83*, 801−805.
(43) Eslava, S.; Zhang, L.; Esconjauregui, S.; Yang, J.; Vanstreels, K.; Baklanov, M. R.; Saiz, E. *Chem. Mater.* **2013**, *25*, 27−33.
(44) Brivio, F.; Walker, A. B.; Walsh, A. *APL Mater.* **2013**, *1*, 042111.
(45) Kresse, G.; Furthmüller, J. *Phys. Rev. B: Condens. Matter Mater. Phys.* **1996**, *54*, 11169.
(46) Perdew, J. P.; Ruzsinszky, A.; Csonka, G. I.; Vydrov, O. A.; Scuseria, G. E.; Constantin, L. A.; Zhou, X.; Burke, K. *Phys. Rev. Lett.* **2008**, *100*, 136406.
(47) Jackson, A. J.; Skelton, J. M.; Hendon, C. H.; Butler, K. T.; Walsh, A. *J. Chem. Phys.* **2015**, *143*, 184101.
(48) Heyd, J.; Scuseria, G. E.; Ernzerhof, M. *J. Chem. Phys.* **2003**, *118*, 8207.
(49) Krukau, A. V.; Vydrov, O. A.; Izmaylov, A. F.; Scuseria, G. E. *J. Chem. Phys.* **2006**, *125*, 224106.
(50) Butler, K. T.; Hendon, C. H.; Walsh, A. *J. Am. Chem. Soc.* **2014**, *136*, 2703−2706.
(51) https://github.com/WMD-Bath/MacroDensity (accessed May 24, 2016).
(52) Blum, V.; Gehrke, R.; Hanke, F.; Havu, P.; Havu, V.; Ren, X.; Reuter, K.; Scheffler, M. *Comput. Phys. Commun.* **2009**, *180*, 2175−2196.
(53) Momma, K.; Izumi, F. *J. Appl. Crystallogr.* **2011**, *44*, 1272−1276.

DOI: 10.1021/acs.inorgchem.6b00979
Inorg. Chem. 2016, 55, 7265−7269